Journal of Electroanalytical Chemistry 753 (2015) 35–41

Contents lists available at ScienceDirect

Journal of Electroanalytical Chemistry

journal homepage: www.elsevier.com/locate/jelechem

The role of re-aggregation on the performance of electrochemically exfoliated many-layer graphene for Li-ion batteries

Christopher Sole [a], Nicholas E. Drewett [a], Fei Liu [b], Amr M. Abdelkader [b], Ian A. Kinloch [b], Laurence J. Hardwick [a,*]

[a] Stephenson Institute for Renewable Energy, Department of Chemistry, The University of Liverpool, Crown Street, Liverpool L69 7ZD, UK
[b] School of Materials, University of Manchester, Manchester M13 9PL, UK

ARTICLE INFO

Article history:
Received 19 November 2014
Received in revised form 28 April 2015
Accepted 9 May 2015
Available online 15 May 2015

Keywords:
In situ Raman microscopy
Li-ion battery
Graphite electrode
Exfoliation
Restacking

ABSTRACT

Two potential pathways for Li^+ diffusion occur within graphitic carbon with typically in-plane diffusion dominating ($\sim 10^{-7}$ cm^2 s^{-1}) over diffusion along the crystallite grain boundaries ($\sim 10^{-11}$ cm^2 s^{-1}). Reducing the flake thickness of microcrystalline graphite powders via electrochemical exfoliation offers a method to overcome the latter, sluggish grain boundary Li^+ diffusion, thereby increasing the overall rate capability of the graphite negative electrode in a the Li-ion battery. Six micron particulate graphite was electrochemically exfoliated to give flakes of which ~90% had a thickness of <10 graphene layers. This exfoliated material was then prepared as an ink and allowed to dry prior to forming a battery electrode. Analysis of the electrode and dried exfoliated powder using powder X-ray diffraction, scanning electron microscopy and Brunauer–Emmett–Teller isotherm analysis show that the material has, apart from a significant reduction of the rhombohedral fraction from 41% to 14%, near-identical properties to that of original starting graphite powder. Thus, once the exfoliated powder has been dried from the exfoliation process, as anticipated, major restacking of the multi-layer graphene flakes had occurred. Likewise there was no significant improvement in using the exfoliated material at high rates of delithiation and lower specific capacity, when tested within a half cell vs. lithium metal. *In situ* Raman analysis showed that the exfoliated material displayed similar spectral features to the pristine sample during lithiation, as did multi point measurements on differently disordered areas shown from the varying I_D/I_G-band intensity ratios, indicating that local surface disorder does not influence the course of lithium insertion. The re-aggregation of graphenic material is widely recognised, but seldom evaluated. This work shows the importance of keeping graphenic material dispersed at all stages of production.

1. Introduction

There are presently no guidelines for designing carbon-based electrode architectures for lithium-ion batteries, particularly for high-power applications. A prospective avenue of development would be to modify or fabricate graphitic flakes to take best advantage of their Li^+ diffusion properties. It has been reported that Li^+ diffusion through graphitic carbon can occur via two pathways: typically in plane diffusion dominates ($\sim 10^{-7}$ cm^2 s^{-1}) over diffusion along the crystallite the grain boundaries ($\sim 10^{-11}$ cm^2 s^{-1}) (Fig. 1a) [1]. A design that efficiently utilises the fast in-plane lithium diffusivity has been previously postulated. It is based upon graphitised natural graphite (MCMB – mesocarbon microbeads) with a typical crystalline domain size of around 45 nm, which could be intercalated/deintercalated in less than 0.2 ms [1]. Such a rate would compete with the fastest-rate cathode materials seen to date [2]. As described, a rate-promoting design could potentially be achieved by creating graphite particles with radially aligned crystallites, where the graphene planes are parallel to each other in radial direction. Herein we present work towards a different concept to generate very thin high aspect ratio graphitic flakes in order to overcome sluggish grain boundary diffusion of Li^+. Reductive electrochemical exfoliation has been shown to be an effective method in generating single and multi-layer graphene sheets greater than one micron diameter [3–5]. In this method tetraalkylammonium cations are electrochemically inserted into graphitic carbons in order to exfoliate them to produce flakes down to a monolayer. As the method is reductive, the resultant flakes have low oxygen content, and therefore are of potential interest for Li-ion negative electrodes.

* Corresponding author.
E-mail address: hardwick@liverpool.ac.uk (L.J. Hardwick).

http://dx.doi.org/10.1016/j.jelechem.2015.05.011
1572-6657/

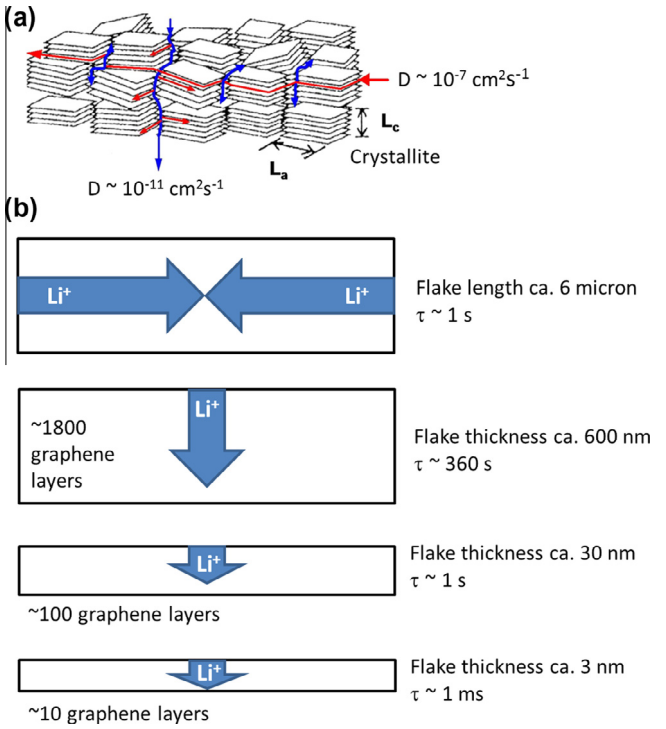

Fig. 1. (a) Figure showing the diffusion pathways of Li^+ through a graphite particle (b) design principle and diffusion times for higher rate graphitic particles from controlling flake thickness.

Fig. 1a illustrates an idealised picture of a graphitic particle comprised of crystallites with lateral and thickness dimensions of L_a and L_c respectively. The effect of anisometric Li^+ diffusion on diffusion times with respect to particle dimensions is shown in Fig. 1b. Li^+ diffusion time, τ is calculated by $\tau = L^2/D$, where D is the diffusion coefficient ($cm^2\,s^{-1}$) and L is the diffusion length (cm). Thus, for a particle with an aspect ratio of 10:1 where the particle length is 6 μm and thickness is 600 nm, the Li^+ diffusion time along grain boundaries is 360 times slower than between the graphene sheets. Reducing the particle thickness will allow Li^+ diffusion through grain boundary pathways to become more significant. Thereby decreasing the thickness down to 100 graphene layers brings parity of the diffusion times, and reducing further to 10 layers decreases the grain boundary diffusion time to 1000× faster than between the graphene sheets. In this paper the effect of modification of synthetic graphite via reductive exfoliation on structure is studied and the resultant Li electrochemistry is presented.

It is however, acknowledged that graphenic material re-aggregates, if allowed to dry out. It is the intension of this paper to characterise the structural changes that have occurred during exfoliation and subsequent restacking. As well as to examine whether such rearrangements have any significant effect on electrochemical performance of the material, as the active component of a Li-ion battery negative electrode, via the introduction of stacking faults that may provide shorter grain boundary diffusion path lengths.

2. Experimental

2.1. Electrochemical reduction method for producing exfoliated graphite and Raman characterisation of product

The experimental setup and process for electrochemical exfoliation of graphite is illustrated in Fig. 2. A two electrode system was used for the process, a ca. 6 micron-sized synthetic graphite carbon SFG6 (Timcal, AG) was selected and pressed into a pellet and used as working electrode, the electrolyte was composed of dimethyl sulfoxide (DMSO) saturated with lithium chloride (LiCl) and triethylammonium hydrochloride (Et_3NHCl), and a graphite rod was used as counter electrode. A negative voltage (−10 V) was applied to the working electrode for 8 h, during this process the graphite pellet dissociated and spread into the solution due to the intercalation of Li^+ and triethylammonium ions [3]. Afterwards, the exfoliated graphitic material was dispersed in water, then collected by vacuum filtration and washed repeatedly with water to remove the residual ions. Finally, the obtained powder was dried in an electric oven at 80 °C for 5 h to ensure that the sample was completely moisture free to prevent any hydration of the lithium in the battery testing. This process can be repeated to achieve a higher exfoliation level.

2.2. Characterisation of graphite powders

Powder X-ray diffraction (PXRD) data were collected on a Bruker D8 Advance operating in transmission mode with a copper source (λ = 1.5418 Å). The average crystallite size along the crystallographic *c*-axis (L_c) and the *a*-axis directions (L_a) were determined from the XRD data by peak fitting the (100) and the (002) peaks for both the SFG6 and the exfoliated-SFG6.

These peaks were then analysed using the Scherrer equation:

$$L\,(\mathrm{nm}) = \frac{K\lambda}{\beta\cos\theta} \qquad (1)$$

where L is the average crystallite size along the analysed plane, K (the dimensionless shape factor) is a constant (here 0.9), λ is the wavelength of the X-rays, θ is the Bragg diffraction angle of the analysed plane and β is the full width at half-maximum (FWHM) of the analysed peak. By determining L for the (100) and (002) fitted peaks, it was possible to determine the values for L_a and L_c respectively. The rhombohedral fraction (3R phase) was then determined by comparison of the ratio of the intensities of the (101) hexagonal and rhombohedral diffraction peaks. Relative surface disorder was determined via Raman spectroscopy from the average intensity ratio of D and G bands (I_D/I_G) of the graphite powders taken from 400 points on the powder surface across an area of 95 μm × 95 μm. Surface area measurements were conducted using a Quantachrome NOVA 4200e Volumetric Gas Sorption Analyser, employing high purity nitrogen (99.9995) at 77.35 K. Approximately 400 mg of each of the powders were degassed overnight at 350 °C to 10^{-3} mbar dynamic vacuum. The surface area of the powders were calculated via the multipoint Brunauer–Emmett–Teller (BET) analysis of the isotherm using five data points with relative pressures ranging from 0.1 to 0.3. Graphite powder morphologies were characterised using a JEOL 6610 scanning electron microscope operating at an accelerating voltage of 20.0 keV.

2.3. Electrochemical testing

Composite electrodes were prepared from a slurry of 90 wt.% active material (SFG6, Timcal AG or exfoliated-SFG6) and 10 wt.% poly(vinylidene fluoridehexafluoropropylene) co-polymeric binder (Kynarflex, Arkema) cast onto a copper foil current collector. Typical electrodes had a thickness of ~30 μm and mass loading of 2–3 mg cm^{-2}. CR2032 coin cells were assembled in an argon filled glove box (O_2, H_2O < 1 ppm) with 1 M $LiPF_6$ in EC-DMC (BASF) impregnated glass fibre separators (Whatman) and a Li metal counter electrode.

Electrochemical charge/discharge measurements were carried out at 30 °C (Maccor Series 4200 battery cycler). An asymmetric cycling procedure was developed whereby an initial galvanostatic

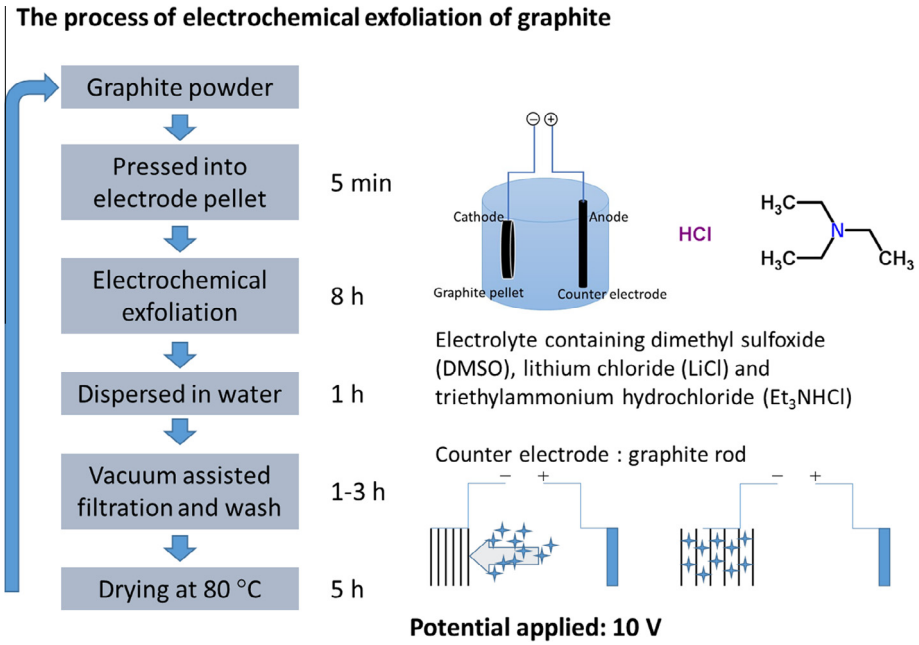

Fig. 2. Electrochemical reduction method for producing exfoliated graphite.

discharge at 10 mA g^{-1} (C/37) down to 0.005 V vs. Li/Li^+ is followed by a potentiostatic step at this potential until the current dropped below 5 mA g^{-1}. This slow rate and potentiostatic step promotes the formation of a stable solid electrolyte interphase (SEI) during the first Li^+ insertion cycle. On delithiation, the cell was charged up to 1.5 V vs. Li/Li^+ at C/37. On subsequent cycles the galvanostatic current was varied to compare rate performance on delithiation, (3 × C/10, then 5 × C, 5C, 10C, 15C, 20C) with a constant slow lithiation rate of 74.4 mA g^{-1} (C/5) to avoid lithium plating.

2.4. In situ Raman measurements

Raman electrodes were prepared by dispersing exfoliated-SFG6, poly(vinylidene fluoride-hexafluoropropylene) co-polymeric binder (Kynar-flex, Arkema) and dibutyl phthalate (Aldrich) in acetone which was then cast onto glass at a thickness of 60 μm. Once dry, the free-standing film was removed from the glass plate with the dibutyl phthalate plasticiser extracted using diethyl ether, after which 4 mm diameter electrodes punched from the cast. These were dried under vacuum at 90 °C, weighed and then transferred to an argon filled glovebox (O_2, H_2O < 1 ppm) for Raman cell assembly. The loadings of the electrodes were 3.5 mg cm^{-2}, with a typical electrode mass being ca. 0.5 mg.

The electrodes were used as active material within an *in situ* Raman cell (ECC-Opto-Std, El-Cell) configured as used in previous studies [6], in which the cell assembly is described. Raman spectra were recorded with a Raman microscope (Renishaw inVia), using a 633 nm wavelength laser focussed through a microscope (Leica), via a 50× objective (Leica). The cell had an open circuit potential ca. 2.7 V and spectra were recorded by stepping to different potentials using a potentiostat (Biologic). The potential was decreased at a scan rate of 1 mV s^{-1} and held at 0.4, 0.2, 0.18, 0.15, 0.11 and 0.08 V until a quasi-equilibrium current was reached (<30 mA g^{-1}).

3. Results and discussions

Raman spectroscopy is well known as a versatile technique capable of identifying graphene and determining the number of layers [7]. Fig. 3(a) shows spectra for SFG6 before exfoliation and a typical flake after exfoliation recorded using a laser excitation of 633 nm. The *G* (1581 cm^{-1}) and 2*D* (~2700 cm^{-1}) bands are clearly visible in both cases. Although the position of the 2*D* peak does not shift to a lower wavenumber after exfoliation, the disappearance of the shoulder peak, which is a characteristic of graphite with layer numbers of more than 10, indicates the thickness of the SFG6 particles was reduced after exfoliation and that graphite with layer numbers less than 10 was produced by this process [7,8]. The histogram in Fig. 3(b) shows the change of product with increasing exfoliation cycle numbers (the results obtained by randomly measuring 20 flakes using Raman spectroscopy). The extent of exfoliation increased with number of exfoliation cycles. After 3 cycles, the percentage of flakes less than 10 layers can achieve 90%, and this sample was selected for material, electrochemical and *in situ* Raman characterisation. It also should be noted that the starting graphite material strongly influences the degree of exfoliation achieved as well the final flake size (e.g. HOPG does not exfoliate into individual flakes). The SFG6 material used herein exfoliated reasonably but not as well as some of the other graphite materials we have investigated.

The surface area of the exfoliated-SFG6 was found to be 21 $m^2 g^{-1}$ (Table 1), which is comparable to the starting SFG6 material (22 $m^2 g^{-1}$) and to previous reports on this material [9]. It should be noted that this surface area is typical for solvent exfoliated graphene which has been extensively dried and not re-dispersed, with our laboratory finding a similar surface area for dried few-layer graphene made by the ultrasonic routes developed by Coleman et al. [10].

This indicates that as anticipated, significant restacking of the many-layer graphene material occurred during the drying out of the dispersed powder ink, even before the electrode preparation stage. This is further supported by comparing SEM images (Fig. 4) of SFG6 and exfoliated SFG6, which show no major differences from visual inspection between the two powders. Analysis of the PXRD patterns of the SFG6 and exfoliated-SFG6 (Fig. 5) shows a slight decrease of crystallite size ca. 10–15% in L_a and L_c directions after the electrochemical exfoliation. Most significant is the major decrease in the rhombohedral phase from 41% to

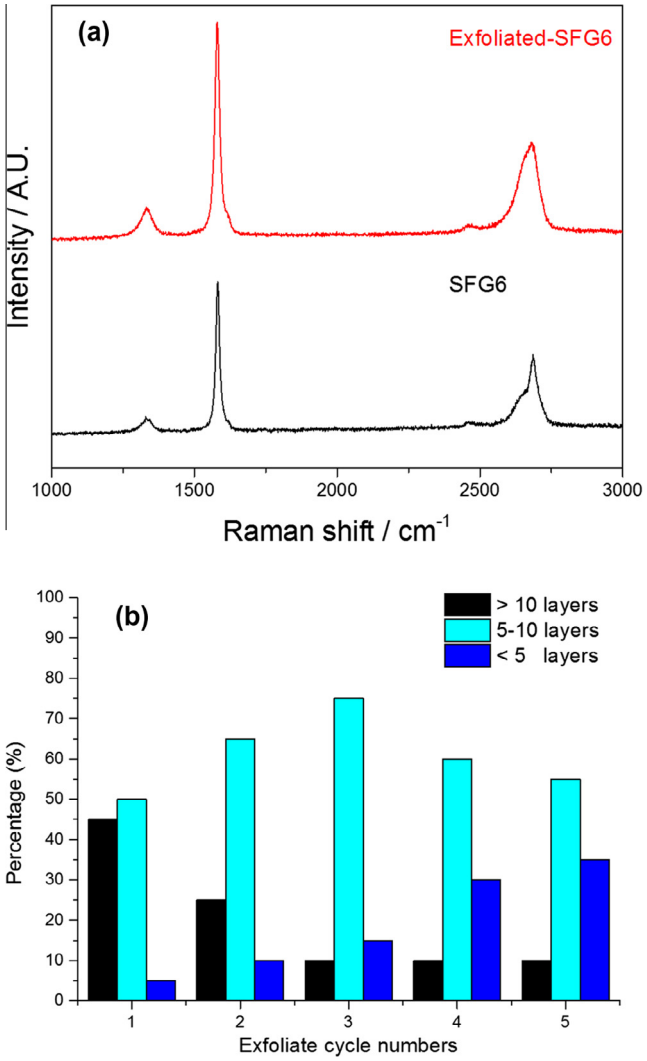

Fig. 3. (a) Example Raman spectrum and (b) distribution of layered materials after randomly measuring 20 pieces of flakes by Raman spectroscopy, via analysis of 2D band.

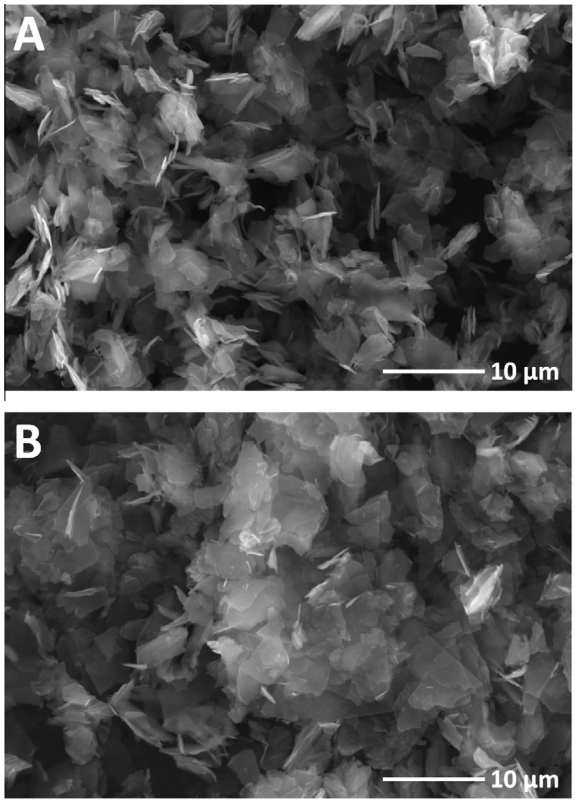

Fig. 4. SEM of (a) SFG6 powder and (b) exfoliated-SFG6.

14%, indicating that the flakes restacked preferentially to the hexagonal form (ABABAB), rather than the rhombohedral (ABCABC) arrangement. Raman mapping analyses of the SFG6 and exfoliated-SFG6 powders show that the surface disorder (I_D/I_G) increases moderately from 0.44 to 0.48, indicating that the exfoliation process has not significantly increased surface disorder. The absence of significant surface disordering of the exfoliated-SFG6 is corroborated by electrochemical testing that demonstrates that the irreversible first cycle charge loss increases from 22% to 28%. Fig. 6 shows that there is no measurable improvement between the cycle rate data for SFG6 and exfoliated-SFG6. This is to be expected given the extent of flake restacking resulting in graphite with similar properties. Exfoliated-SFG6 has a lower capacity at the C/5 rate of 320 mAh g^{-1} vs. 360 mAh g^{-1} indicating that some carbon structures (ca. 10%) produced during restacking may include some turbostratic graphite that is inactive towards Li^+ insertion. Shi et al. [11] found that strains and defects in turbostratically stacked layers cause adjacent layers, to some degree, to lock together and become difficult to move with respect to one another. Consequently, the restraining of these layers prevents the lithium from intercalating into the regions of defective stacking. At higher rates the capacity retention of SFG6 and exfoliated-SFG6 is identical indicating that the active layers present within exfoliated-SFG6 retain the original capacity of the starting material.

The *in situ* Raman microscopy results from the first lithium intercalation into exfoliated-SFG6 are shown in Fig. 7. The first order and second order *in situ* Raman spectra during lithium insertion are in good agreement with literature [6,12–16]. At open circuit potential (ca. 2.7 V vs. Li/Li^+), five distinct bands are observed in the region between 1200 and 2900 cm^{-1}: the *D* band at 1332 cm^{-1}, the *G* band at 1581 cm^{-1}, *D′* at 1616 cm^{-1}, $D + D''$ at 2464 cm^{-1} and the 2*D* band centred at ~2700 cm^{-1}, with 2*D*(1) and 2*D*(2) components at 2649 and 2688 cm^{-1} respectively. At 0.2 V the formation of the dilute stage 1 is observed from the blue-shift of the *G* band from 1581 to 1590 cm^{-1} (Table 2). Below 0.2 V the formation of low stage number compounds begins

Table 1
Structural bulk parameters, surface properties and results of the electrochemical charge/discharge measurements (1st cycle irreversible charge losses) of SFG6 and exfoliated-SFG6 in 1 M $LiPF_6$, 1:1 EC:DMC (*w*:*w*).

	BET (m^2g^{-1})	L_a (Å)	L_c (Å)	I_D/I_G	Rhombohedral 3R-phase	Irreversible charge loss [1st cycle] (%)
SFG6 [9]	17.1	622	303	0.36	37	20
SFG6 (this work)	22	817	797	0.44	41	22
Exfoliated-SFG6	21	764	685	0.48	14	28

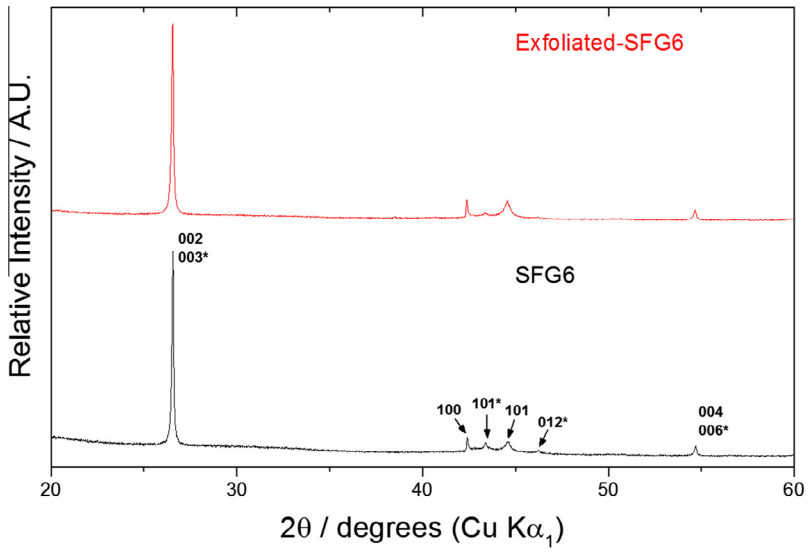

Fig. 5. PXRD of SFG6 and exfoliated-SFG6, ∗ indicates rhombohedral phase.

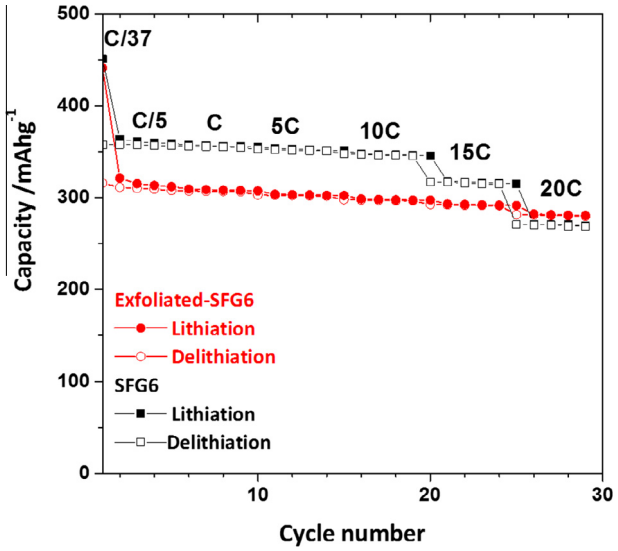

Fig. 6. Rate performance of SFG6 and exfoliated-SFG6.

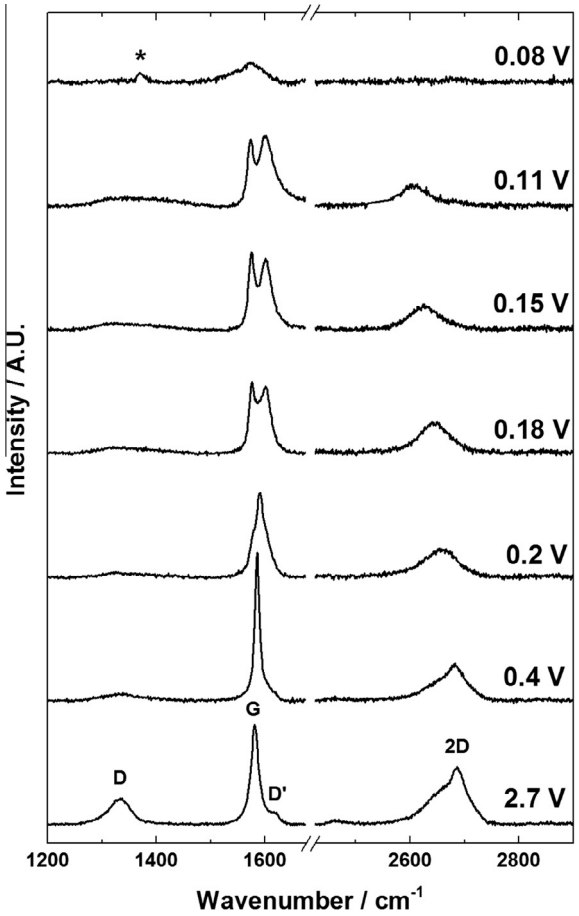

Fig. 7. Representative *in situ* Raman spectra of first cycle lithium intercalation into exfoliated-SFG6. The potential (V) at which each spectrum was collected is displayed. All the spectra are base-line corrected and stacked arbitrarily up the *y*-axis to allow for clear visualisation. ∗ indicates possible shifted E_{2g2} phonon (1371 cm^{-1}).

and is realised by 0.18 V with the appearance of the E_{2g2}(i) (1576 cm^{-1}) and E_{2g2}(b) (1601 cm^{-1}) bands. By 0.08 V the doublet structure is no longer observed, with the presence of band at 1371 cm^{-1} and a broad band centred at 1572 cm^{-1}. The 1572 cm^{-1} feature indicates the formation of a stage 2 intercalation compound. The band at 1371 cm^{-1} has been observed previously and its origin remains poorly understood [6]. However recent inelastic X-ray scattering measurements have shown that the E_{2g2} phonon (*G* band) for LiC_6 softens all the way to ~1380 cm^{-1} as the electron doping destabilises the C–C bonds [17] and therefore the observed band at 1371 cm^{-1} could be this measured phonon mode. The *D* band intensity decreases as the potential is lowered and by 0.2 V is challenging to accurately peak-fit, once the sloping background has been removed. The *D′* (1616 cm^{-1}) and $D + D''$ (2464 cm^{-1}) though clearly evident at 2.7 V, by 0.2 V have decreased in intensity to be no longer discernible above the back ground noise.

The 2*D* band changes shape and shifts with potential, as previously reported [6] (Fig. 7 and Fig. 8). The fitted 2*D*(1) and 2*D*(2) band positions remain fairly constant until 0.4 V (Table 2). The 2*D* peak changes shape below 0.4 V, and at 0.2 V the 2*D*(1) peak is no longer resolved leaving the single 2*D*(2) band (2655 cm^{-1}). Between 0.2 and 0.11 V the 2*D*(2) peak shifts from 2658 to

Table 2
In situ Raman peak positions (cm^{-1}) and full width at half maximum (FWHM) (cm^{-1}) of first electrochemical lithium insertion into exfoliated-SFG6.

E/V vs. Li/Li^+	*D*	*G*	*D′*	*D* + *D″*	2*D*(1)	2*D*(2)
2.7	1332 (42)	1581 (17)	1616 (17)	2464 (23)	2649 (54)	2688 (36)
0.4	1336 (66)	1585 (10)	1605 (18)	2461 (16)	2646 (54)	2683 (39)
0.2	–	1591 (24)	–	–	–	2655 (67)
0.18	–	E_{2g2}(i) 1576 (13) E_{2g2}(b) 1600 (22)	–	–	–	2644 (59)
0.15	–	E_{2g2}(i) 1575 (11) E_{2g2}(b) 1601 (25)	–	–	–	2626 (59)
0.11	–	E_{2g2}(i) 1573 (10) E_{2g2}(b) 1602 (34)	–	–	–	2607 (56)
0.08	–	1371 (13) 1572 (48)	–	–	–	–

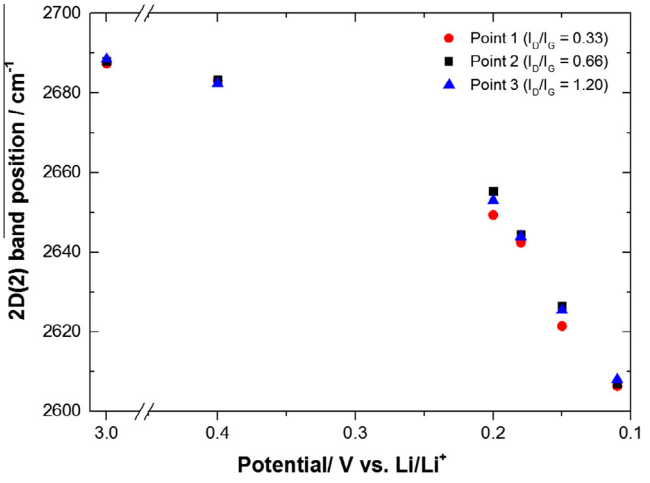

Fig. 8. The shift in 2D(2) position within potential range 3.0–0.15 V vs. Li/Li^+ for the first lithiation of exfoliated-SFG6 of three points with varying initial I_D/I_G ratios.

2607 cm^{-1}, and at 0.08 V the 2*D*(2) band is no longer present. This is because the electronic doping of the systems is to such the extent that it now fully disallows the activation of the double resonance band. Fig. 8 shows the 2*D*(2) peak shift measured at different points on the electrode under potential control, with the points having I_D/I_G ratios of 0.33, 0.66 and 1.2. The 2*D* band shift for each of these points are 497 ± 47, 541 ± 18 and 509 ± 26 cm^{-1} V^{-1} respectively. The similarity of the shift indicates that local graphitic disorder does not have any influence on the behaviour of the 2*D* band during lithium insertion.

4. Conclusions

Producing few- and many- layer graphene on a large scale, where the flake sizes are greater than 1 μm, remains non-trivial. The reductive electrochemical exfoliation method offers a promising approach to overcome this challenge, and in particular tailor graphitic particles for Li-ion negative electrodes. 6 μm diameters, particulate graphite were reductively electrochemically exfoliated to give flakes of which ~90% were thinner than 10 layers. However it was found that restacking of the flakes is a major consideration when the produced material is allowed to dry out. PXRD shows significant reduction of rhombohedral fraction has occurred during the restacking of the multi and few-layer graphene flakes produced, as well as a measured lower initial specific capacity (ca. 320 mAh g^{-1}) resulting from partial turbostratic formation during the restacking. *In situ* Raman microscopy of the exfoliated-SFG6 shows similar electrochemical and spectroscopic behaviour to SFG6, indicating that exfoliation process and subsequent restacking has had no influence on Li insertion. The 2*D* band shift during stage formation is not influenced by the initial level of disorder (I_D/I_G), suggesting that the measured 2*D* shift is predominantly due to electron doping rather than being structural in origin. Future work is focussing on the production of the electrodes from exfoliated material using routes to prevent re-aggregation at the ink stage in order to construct high rate performing graphite electrodes.

Acknowledgement

We acknowledge the Engineering and Physical Sciences Research Council (EPSRC) for the funding of this research under Grant Numbers EP/K016954 and EP/I023879/1.

References

[1] K. Persson, V.A. Sethuraman, L.J. Hardwick, Y. Hinuma, Y.S. Meng, A. van der Ven, V. Srinivasan, R. Kostecki, G. Ceder, Lithium diffusion in graphitic carbon, J. Phys. Chem. Lett. 1 (2010) 1176–1180.
[2] B. Kang, G. Ceder, Battery materials for ultrafast charging and discharging, Nature 458 (2009) 190–193.
[3] A.M. Abdelkader, I.A. Kinloch, R.A.W. Dryfe, Continuous electrochemical exfoliation of micrometer-sized graphene using synergistic ion intercalations and organic solvents, ACS Appl. Mater. Interfaces 6 (2014) 1632–1639.
[4] A.J. Cooper, N.R. Wilson, I.A. Kinloch, R.A.W. Dryfe, Single stage electrochemical exfoliation method for the production of few-layer graphene via intercalation of tetraalkylammonium cations, Carbon 66 (2014) 340–350.
[5] A.J. Cooper, M. Velicky, I.A. Kinloch, R.A.W. Dryfe, On the controlled electrochemical preparation of R_4N^+ graphite intercalation compounds and their host structural deformation effects, J. Electroanalyt. Chem. 730 (2014) 34–40.
[6] C. Sole, N.E. Drewett, L.J. Hardwick, In situ Raman study of lithium-ion intercalation into microcrystalline graphite, Faraday Discuss. 172 (2014) 223–237.
[7] A.C. Ferrari, D.M. Basko, Raman spectroscopy as a versatile tool for studying the properties of graphene, Nat. Nanotechnol. 8 (2013) 235–246.
[8] A.C. Ferrari, J.C. Meyer, V. Scardaci, C. Casiraghi, M. Lazzeri, F. Mauri, S. Piscanec, D. Jiang, K.S. Novoselov, S. Roth, A.K. Geim, Raman spectrum of graphene and graphene layers, Phys. Rev. Lett. 97 (2006).
[9] H. Buqa, A. Wursig, D. Goers, L.J. Hardwick, M. Holzapfel, P. Novák, F. Krumeich, M.E. Spahr, Behaviour of highly crystalline graphites in lithium-ion cells with propylene carbonate containing electrolytes, J. Power Sources 146 (2005) 134–141.
[10] Y. Hernandez, V. Nicolosi, M. Lotya, F.M. Blighe, Z. Sun, S. De, I.T. McGovern, B. Holland, M. Byrne, Y.K. Gun'Ko, J.J. Boland, P. Niraj, G. Duesberg, S. Krishnamurthy, R. Goodhue, J. Hutchison, V. Scardaci, A.C. Ferrari, J.N. Coleman, High-yield production of graphene by liquid-phase exfoliation of graphite, Nat. Nanotechnol. 3 (2008) 563–568.
[11] H. Shi, J. Barker, M.Y. Saidi, R. Koksbang, Structure and lithium intercalation properties of synthetic and natural graphite, J. Electrochem. Soc. 143 (1996) 3466–3472.
[12] L.J. Hardwick, H. Buqa, M. Holzapfel, W. Scheifele, F. Krumeich, P. Novák, Behaviour of highly crystalline graphitic materials in lithium-ion cells with propylene carbonate containing electrolytes: an in situ Raman and SEM study, Electrochim. Acta 52 (2007) 4884–4891.
[13] W.W. Huang, P. Frech, In situ Raman studies of graphite surface structures during lithium electrochemical intercalation, J. Electrochem. Soc. 145 (1998) 765–770.

[14] M. Inaba, H. Yoshida, Z. Ogumi, T. Abe, Y. Mizutani, M. Asano, In-situ Raman-study on electrochemical Li-intercalation into graphite, J. Electrochem. Soc. 142 (1995) 20–26.
[15] P. Lanz, P. Novák, Combined in situ Raman and IR microscopy at the interface of a single graphite particle with ethylene carbonate/dimethyl carbonate, J. Electrochem. Soc. 161 (2014) A1555–A1563.
[16] L.J. Hardwick, H. Buqa, P. Novák, Graphite surface disorder detection using in situ Raman microscopy, Solid State Ionics 177 (2006) 2801–2806.
[17] A. Walters, M. Dean, C. Howard, M. Ellerby, J. Payne, M. Krisch, A. Bosak, G. Profeta, M. Calandra, F. Mauri, Understanding electron-phonon interactions in doped graphene: the case of Li-intercalated graphite, Am. Phys. Soc. Abstracts 57 (2012).